Gaussian Masked Autoencoders

Jathushan Rajasegaran[1,2]**, Xinlei Chen**[1]**, Rulilong Li**[2]**,**
Christoph Feichtenhofer[1]**, Jitendra Malik**[1,2]**, Shiry Ginosar**[3]
Meta, FAIR[1], UC Berkeley[2], Toyota Technological Institute at Chicago[3]

Abstract

This paper explores Masked Autoencoders (MAE) with Gaussian Splatting. While reconstructive self-supervised learning frameworks such as MAE learns good semantic abstractions, it is not trained for explicit spatial awareness. Our approach, named Gaussian Masked Autoencoder, or GMAE, aims to learn semantic abstractions and spatial understanding jointly. Like MAE, it reconstructs the image end-to-end in the pixel space, but beyond MAE, it also introduces an intermediate, 3D Gaussian-based representation and renders images via splatting. We show that GMAE can enable various zero-shot learning capabilities of spatial understanding (*e.g.*, figure-ground segmentation, image layering, edge detection, *etc.*) while preserving the high-level semantics of self-supervised representation quality from MAE. To our knowledge, we are the *first to employ Gaussian primitives in an image representation learning framework* beyond optimization-based single-scene reconstructions. We believe GMAE will inspire further research in this direction and contribute to developing next-generation techniques for modeling high-fidelity visual data. More details at https://brjathu.github.io/gmae.

1 Introduction

Vision systems, by nature, process raw, low-level observations of the world, but visual reasoning frequently requires spatial understanding as well as higher-level semantic abstractions of the data. In this work, we aim to learn the structure of the world, which is constructed from objects and their relationships in 3D space. We learn these abstractions from raw image observations by learning masked auto-encoders controlled by 3D Gaussians as their intermediate representations.

What sort of spatial understanding does visual reasoning require? In this work, we take inspiration from Wang and Adelson (Wang & Adelson, 1994), who demonstrated that the simplest version of a spatially-aware representation consisting of 2.1D layers is sufficient for representing objects that inherently move with respect to one another. Even in static images, layered representations allow us to learn more about the structure of the world (Tucker & Snavely, 2020; Zhou et al., 2018). We, therefore, set ourselves the task of learning image representations that are both layered and at the level of abstraction of single objects.

Learning high-level semantic abstractions can be achieved by supervised learning (Krizhevsky et al., 2012; He et al., 2015; Dosovitskiy et al., 2020) or by learning binding from large scale paired datasets (Radford et al., 2021; Jia et al., 2021; Zhang et al., 2022; Rombach et al., 2022). However, self-supervised learning has recently emerged as the more promising approach in this direction (Oquab et al., 2024; Grill et al., 2020; Bao et al., 2021; He et al., 2022; Wei et al., 2022). Notably, Masked Autoencoders (MAE) (He et al., 2022) demonstrated that self-supervised learning is an effective representation learning mechanism by directly predicting the RGB values of masked image patches. However, while the leading methods, such as MAE (He et al., 2022) and DINOv2 (Oquab et al., 2024), learn higher-level representations of images, they are not trained for explicitly recovering the spatial structure of objects and scenes in the world.

This paper proposes jointly learning high-level semantic abstractions such as objectness, grouping, and semantic structure with 2.1D layering via self-supervised learning. Our idea is conceptually simple: given MAE, a pixel-based self-supervised representation learning approach, we design mechanisms that can lead to desirable intermediate representations as *learned* latents. Specifically, our central insight is that 3D Gaussians (Kerbl et al., 2023) are a good candidate for intermediate image representations that can lead to semantic and spatial understanding.
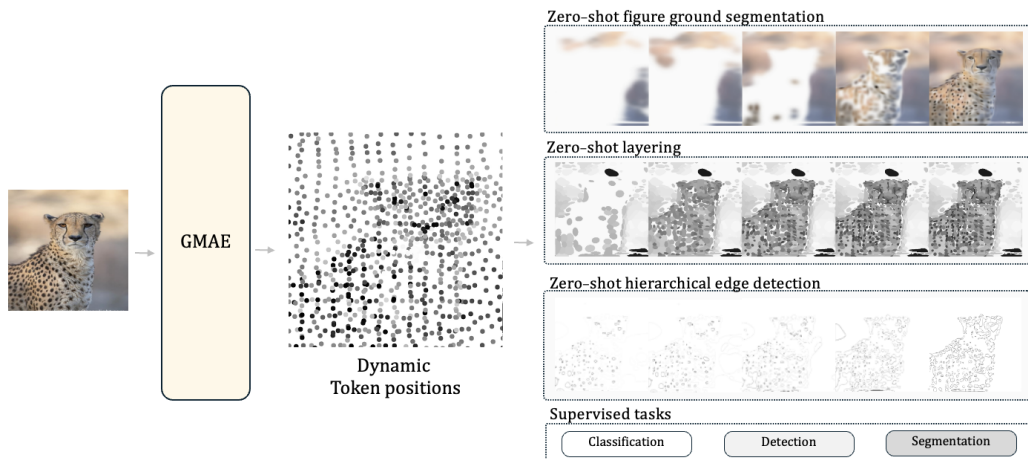
Figure 1: **Gaussian Masked Autoencoders (GMAE)** maintains high performance in supervised representation learning tasks such as classification, detection, and segmentation, but more importantly enables zero-shot capabilities. GMAE introduces a learned mid-level intermediate representation of 3D Gaussians that we train using pixel-based image reconstruction losses rather than direct supervision by rendering the Gaussians into pixel space. Through this reconstruction loss, the Gaussian collection learns to distribute non-uniformly in space and scale, dynamically following the input image's information density and high-frequency details. Having the degree of freedom in depth allows the model to learn the layering of objects and scenes, which enables figure-ground separation, layering, and edge detection without any training.

3D Gaussians were initially proposed for optimization-based 3D reconstruction. Different from geometrically uniform representations like square pixel patches, their size, location, and information distribution over the image are dynamically learned. Moreover, Gaussian-based representations could lend themselves to end-to-end learning thanks to splatting image rendering (Kerbl et al., 2023) that maps them back to the pixel space. We can, therefore, jointly learn such a mid-level representation within self-supervised frameworks such as MAE. We name our approach Gaussian Masked Autoencoders, or GMAE. To the best of our knowledge, *we are the first to explore such Gaussian primitives in a visual representation learning framework*, rather than an optimization-based 3D reconstruction framework for single scenes. Our approach adds only a negligible overhead compared to standard MAE training – the addition of splatting increases compute time by 1.5%. Without compromising representation-learning performance, GMAE gains significant wins in zero-shot capabilities.

Fig. 1 shows several built-in advantages of a Gaussian-based image representation. First, we note that the non-uniformity of the representation leads to a spatial distribution of representational density that correlates with the information density in the image. By allowing the 3D Gaussians to move along the z-axis, our model learns underlying structure of the natural world by observing not only the single viewpoint of one image but millions of such single views. As a result, we can find figure-ground segmentation, simple layering, and edge detection as depth discontinuity without any tuning.

Besides these advantages, we show that the representations learned with GMAE perform similarly to MAE on image classification and object detection tasks. The representation quality improves with the number of Gaussians used. These results suggest GMAE *augments* MAE and can serve as a better alternative in applications that can benefit from using mid-level representations. The advantage of GMAE becomes apparent when considering that splatting-based rendering is highly efficient, and our current training is *almost as fast as* vanilla MAE baselines.

We hope our exploration can inspire further research along this hybrid direction for representation learning: the reconstruction target is grounded to pixels while jointly learning effective high-level semantic abstractions and spatial understanding with mid-level representations for images. We believe it can contribute to the next generation of techniques for modeling high-fidelity visual data.

2 RELATED WORK

Self-supervised Learning: Over the years, self-supervised pre-training has proven effective in many areas, including language, vision, and robotics. In computer vision, there are two primary schools of thought: discriminative and reconstructive pre-training with visual data. Discriminative pre-training involves training an instance discrimination model to learn the similarity between different augmented image versions. Wu et al. (2018) and SimCLR (Chen et al., 2020) showed that instance discrimination training can be used to learn strong discriminative features via contrastive learning. Later, notable works such as MoCo (He et al., 2020) and DINO (Caron et al., 2021) have shown the effectiveness of such trained visual representations for various downstream tasks.

Reconstructive pre-training learns to model the data distribution by trying to reconstruct an image or a video from its noisy version. One of the most successful methods for such pre-training in computer vision has been the BERT (Devlin et al., 2018)-style masked modeling of images proposed by BEiT (Bao et al., 2021), and MAE (He et al., 2022). Compared to BERT, MAE uses asymmetric encoder-decoders, allowing it to be very efficient at training with high masking ratios. This style of reconstructive pre-training learns strong visual priors and shows impressive results on various downstream tasks such as object detection (Li et al., 2022), pose estimation (Xu et al., 2022), and robot tasks (Radosavovic et al., 2022).

Mid-level Representations: Image can be constructed by operating functions on some representations. One line of approachs keep the representations in the latent spaces, and use a pretrained decoder network to re-construct the image. VAE (Kingma, 2013) with image synthesis (Rombach et al., 2022; Li et al., 2023) are good examples of this case, along with MAE He et al. (2022) and BEiT Bao et al. (2021). Other line of approaches follow a structured representations to represent an image. There are various such options: super-pixels, Gaussians, SVG code and multi-plane images etc. For example Super-pixel sampling networks (Jampani et al., 2018) learns to predict super-pixels as the representation to reconstruct and to predict segmentations and flow. Multi-plane images is another way to represent an image (Tucker & Snavely, 2020), where an image is composed by multiple layered planes, and can be learned end-to-end. There are hybrid approaches also exist. For example, slot-attention (Locatello et al., 2020), learns an intermediate representation for objects, by adding a bottleneck in the model architecture. Similarly Leopart (Ziegler & Asano, 2022) learns to cluster the patches based on self-supervised clustering. In this paper, we take another approach which uses 3D Gaussians as intermediate representations to reconstruct an image.

Gaussian Splatting: Gaussian splatting (Kerbl et al., 2023) is a novel differentiable volume splatting technique using Gaussian primitives as the 3D representation, offering high optimization flexibility and high fidelity in reconstruction. This idea follows a long list of differentiable rendering techniques that recently gained significant attention as a method to bridge the gap between the 3D world and 2D images. Differentiable rendering allows for reconstructing 3D representations (e.g., meshes, point clouds) from 2D image signals by enabling gradient-based optimization. For example, (Liu et al., 2019) introduces a differentiable rasterizer for meshes using probability aggregation. (Lassner & Zollhöfer, 2021) proposes an efficient and differentiable formula to render large sets of point clouds. (Mildenhall et al., 2021) and (Barron et al., 2022) apply differentiable volume rendering (Levoy, 1990) to reconstruct 3D radiance fields from a handful of multi-view images.

In this paper, we propose that 3D Gaussians are a useful learned mid-level image representation due to their non-uniformity properties. We take advantage of the splatting operation from (Kerbl et al., 2023) that enables end-to-end training of mid-level representations with image-based losses. We then use Gaussian primitives in a representation learning framework rather than a single-scene optimization-based 3D reconstruction as in (Kerbl et al., 2023), thus opening the door for using learned 3D Gaussian representations in computer vision applications.

The key advantages of Gaussian splatting include its ability to adapt to scene complexity, efficient rendering, and high-quality reconstructions. Unlike uniform voxel grids, Gaussian primitives can vary in size and density, allowing for more compact and expressive representations of 3D scenes. This adaptability makes them particularly suitable for a wide range of computer vision tasks, from 3D reconstruction to novel view synthesis and beyond.

3 METHOD

We propose a method that reconciles pixel-based learning, the mainstream in self-supervised learning, and latent-based learning, which can impose extra properties on representations. Our key insight is that end-to-end learnable 3D Gaussians are good candidates for mid-level image representations due to their non-uniform properties. Given a large collection of images, we train a Masked Autoencoder (MAE) (He et al., 2022) to reconstruct full images from their masked inputs. The MAE encoder is a ViT (Dosovitskiy et al., 2020) that learns to encode the visible square patches of the masked images into learned embeddings. However, rather than predicting patches of pixels directly as in MAE (He et al., 2022), our ViT-based decoder predicts explicit 3D Gaussians (Kerbl et al., 2023) — their color, 3D center location, scale, and orientation. We then render these Gaussians as images with a splatting differentiable renderer and train the entire model using an MSE loss in pixel space.

3.1 PRELIMINARIES

Self-supervised Masked Autoencoders. Masking autoencoders model the data distribution by randomly masking parts of the data and predicting the masked parts. In language, BERT (Devlin et al., 2018) is trained by masking part of the text tokens and predicting them using a transformer model (Vaswani et al., 2017). In vision, MAE (He et al., 2022) and BEiT (Bao et al., 2021) mask image patches at the input and predict the masked regions. In MAE (He et al., 2022), a ViT (Dosovitskiy et al., 2020) encoder encodes the visible patches, and a smaller decoder ViT model is used with masked tokens to reconstruct the masked patches.

3D Gaussian Primitives and Splatting. Our model learns a mid-level image representation using the 3D Gaussian primitives originally proposed for optimization-based single-scene 3D reconstruction by (Kerbl et al., 2023). Each Gaussian is characterized by a 3D covariance matrix $\Sigma \in \mathcal{R}^{3 \times 3}$ and a center location $p \in \mathcal{R}^3$. Additionally, each Gaussian is assigned a color $r \in \mathcal{R}^3$ and an opacity $o \in \mathcal{R}$ to encode the scene content. For image rendering, these Gaussian primitives are transformed into camera coordinates and projected onto the image plane using volume splatting. Due to the differentiable nature of this process, the attributes of the Gaussian primitives can receive gradients from the rendered image. In our work, we adopt the standard approach of factorizing the covariance matrix $\Sigma = RSS^T R^T$ into a scaling matrix $S = \text{diag}(s) \in \mathcal{R}^{3 \times 3}$ represented by a scale vector $s \in \mathcal{R}^3$, and a rotation matrix $R \in \mathcal{R}^{3 \times 3}$ represented by a rotation quaternion $\phi \in \mathcal{R}^4$. Consequently, each Gaussian is parameterized by a 14-dimensional vector $g = \{p, s, \phi, r, o\} \in \mathcal{R}^{14}$.

3.2 OUR APPROACH

Our model has a ViT-based encoder model, a lightweight decoder model, and a differentiable renderer. Fig. 2 shows a high-level overview of our method. For a given image, we first patchify it into N patches and randomly mask them with a masking ratio r, resulting in n visible patches. The ViT encoder model only sees the visible patches and encodes them from patches to latent embeddings, $x_i \in \mathcal{R}^{d_{enc}}, i \in \{1, 2, 3, ...n\}$.

Assume the decoder has k learnable query tokens $q_j \in \mathcal{R}^{d_{dec}}, j \in \{0, 1, 2, ...k\}$. Note that k can be any value irrespective of the number of masked tokens. We project the encoder latent to $\hat{x}_i \in \mathcal{R}^{d_{dec}}$ and concatenate it with the query tokens.

$$X_{dec} = \{\hat{x}_i\}_{i=1}^n \cup \{q_j\}_{j=1}^k \tag{1}$$

The decoder sees the X_{dec} tokens and predicts k Gaussians, one for each query token (we discard the predictions for the latent tokens). Each Gaussian is parameterized by a 14-dimensional vector $g_j = \{p, s, \phi, r, o\} \in \mathcal{R}^{14}$.

Once we have k predicted Gaussians, we splat them on a plane with a fixed camera projection and render the splatted Gaussians to generate an image. We limit the size of the Gaussians by using an effective scale $c \cdot \texttt{sigmoid}(s)$. Here, c controls a Gaussian's maximum size. After rendering, we use a mean squared error loss to compare the reconstructed image with the input image on the originally masked pixels.

Note that since the Gaussians are the output of the decoder, they are effectively randomly initialized. This is in contrast to the typical usages of Gaussian splatting for 3D reconstruction that rely on point-cloud initialization. In this work, we do not use any prior knowledge. We directly learn all the Gaussian properties from reconstructing the image.
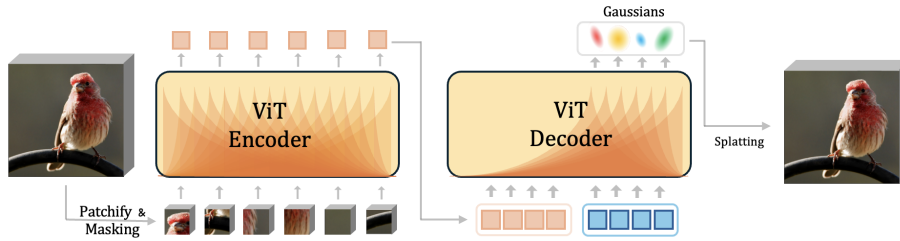
Figure 2: **Masked Autoencoding via Gaussian Splatting:** The ViT Encoder processes masked input image patches to produce latent embeddings . The ViT Decoder then predicts explicit Gaussian parameters based on query tokens , including color, opacity, center, scale, and orientation. These Gaussians are then rendered via differentiable volume splatting (Kerbl et al., 2023) to reconstruct the original image. We pre-train our models fully end-to-end with self-supervision.

4 EXPERIMENTS

4.1 DESIGN CHOICES

First, we will explore various design spaces for pre-training our models. All our experiments in this section are based on a ViT-base encoder and a lightweight decoder and measured by ImageNet (Deng et al., 2009) classification performance. All the models are trained for 400 epochs. We use a base learning rate of $1e-4$ with cosine decay with AdamW (Loshchilov & Hutter, 2017) optimizer. We evaluate our pre-trained models using linear probing and full finetuning.

Number of Gaussians: Unlike MAE, our decoder model is fully decoupled from encoder tokens. Therefore, we can use any number of Gaussians for decoding. We train 4 models that learn to decode 64, 128, 256, and 512 Gaussians, respectively. Fig. 3 shows ImageNet classification performance under linear probing and full fine-tuning as a function of the number of Gaussians. With linear probing, performance monotonically increases as we increase the number of Gaussians. With full fine-tuning, we see a similar behavior at first, but it saturates after 256 Gaussians.
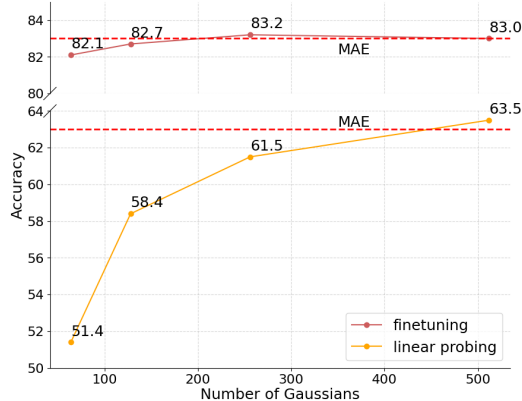

Figure 3: **Number of Gaussians:** ImageNet classification performance with 64, 128, 256, and 512 Gaussians at the decoder during pre-training. We evaluate these models on linear probing and full finetuing. As we increase the number of Gaussians, the performance with linear probing increases monotonically. For full fine-tuning, we see similar behavior at first that saturates after 256 Gaussians.

Gaussian Scale: Since the Gaussians are predictions from the decoder, we can not control their initialization explicitly. We only have an activation function after decoder predictions: for x,y,z we use tanh, and for scale and quaternions we use sigmoid. Since we are learning the scales from randomly initialized Gaussians, we limit the Gaussians from being too big by passing them through the scaled sigmoid function before rendering ($c \times$ sigmoid($scale$)). Here, we study the effect of c on the representation quality. Table 1a shows how classification performance on ImageNet changes by varying the maximum allowed scale values. This essentially controls how big each Gaussian can be and how many pixels they can influence. This variable has only a small effect on the classification performance. However, small scale values greatly hinder the reconstruction quality; see Fig. 4 for qualitative differences.
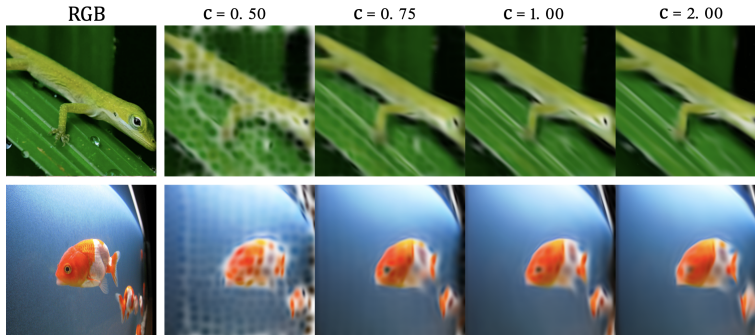
Figure 4: **Effect of scale on reconstruction:** Here we have visualizations to show that With small-scale Gaussians the model can not complete the whole image with a fixed number of Gaussians.

Scale Factor	ft	lin		Masking	ft	lin		Loss	ft	lin
0.50	82.7	61.1		0.70	82.6	60.2		All	81.8	57.4
1.00	**83.2**	**61.9**		0.75	**83.2**	**61.9**		Masked	**83.2**	**61.9**
2.00	83.1	60.9		0.80	82.4	61.9		Masked (norm)	76.9	31.7

(a) Max scale of Gaussians (c)	(b) Masking Ratio	(c) Loss patches

Table 1: **Ablation studies on different model space:** We ablate various configurations for pre-training, including **a)** the maximum allowed scale for a Gaussian, **b)** masking ratio at the encoder, and **c)** which loss is used for pre-training, from applying loss on all patches, only on masked patches to patch-normalized loss. We report classification performance on ImageNet, where higher is better.

Masking Ratio: We study the dependence of our pre-trained models on the masking ratio in Table 1b. MAE (He et al., 2022) showed that higher masking rates allow the model to learn better representations and make the training much more efficient. Using differentiable rendering instead of transformer-based rendering did not change this behavior.

Loss: We also study how to apply the loss on patches. Should we apply on masked patches or all the patches? On pixel prediction or normalized pixel prediction? MAE (He et al., 2022) benefited from predicting normalized patches when applying the loss on masked patches. In our case, a normalized patch loss significantly hurts model performance, as shown in Table 1c. This is due to the fact that all the Gaussians can influence a specific pixel value, a constraint that makes it harder to reconstruct locally normalized patches. Finally, we have a similar observation as in MAE (He et al., 2022); when the loss is applied only to the masked tokens, the model performs slightly better than the model trained with loss applied to all the patches.

Final Model: Based on our findings from the above experiments, our final model is a ViT-base model that is pre-trained with a 0.75 masking ratio for 400 epochs, with patch loss applied to the masked tokens and has 512 Gaussians at the decoder during per-training. We will use this model for the rest of our experiments. All our models are pre-trained on the ImageNet (Deng et al., 2009) 1k dataset.

4.2 SUPERVISED TASKS

To measure the representation quality of our pre-trained models, we evaluate our models on ImageNet-1k (Deng et al., 2009) classification and COCO (Lin et al., 2014) object detection. We use the ViT-base model, trained for 400 epochs with a masking ratio of 0.75, for fine-tuning on ImageNet and COCO.

Image Recognition: Table 2a shows the performance of various pre-trained models on ImageNet classification top-1 accuracy. We fine-tuned our model for 100 epochs, following the protocols of MAE (He et al., 2022). While achieving comparable performance to MAE, our models show an interesting trend when increasing the number of Gaussians, as in Fig. 3. Scaling this further without increasing compute requirements would necessitate further modifications, which we leave for future directions.

Object Detection and Segmentation: As another important way to evaluate our encoder representations, we transfer the representations learned with our pipeline via fine-tuning, to object detection and segmentation. We follow the protocol of ViTDet (Li et al., 2022) and evaluate on the COCO

Method	Top-1
DINO	82.8
BEiT	83.2
MAE (1600-ep)	83.6
MAE (400-ep)	83.0
GMAE (400-ep)	83.2

(a) ImageNet classification.

Method	AP^{box}	AP^{mask}
Supervised	47.6	42.4
MAE (1600-ep)	51.8	44.9
MAE (400-ep)	50.6	45.0
GMAE (400-ep)	50.2	44.5

(b) COCO object detection and segmentation.

Table 2: **GMAE performs comparably to MAE** (He et al., 2022) on supervised tasks.

Figure 5: **Reconstruction Quality:** Examples of test-time reconstructions when the input is fully visible (mask ratio=0). The first row is the RGB images and the second row is our reconstructions. Having a decoupled decoder allows us to perform inference with any masking ratio, even though this model is trained with a 0.75 ratio. The dynamically learned non-uniform spatial and scale distribution of Gaussians enables GMAE to reconstruct high-frequency regions like lines and edges. Our rFID score is 89.45, while MAE rFID is 98.12 (smaller is better), and PSNR of GMAE is 18.74 and of MAE is 18.63.

benchmark (Lin et al., 2014). Again, we find GMAE performs similarly to MAE in AP^{box} and AP^{mask}, and significantly outperforms supervised pre-training. See Table 2b.

4.3 UNSUPERVISED TASKS

In this section, we study the properties of the decoder of our pre-trained models. Unlike MAE, we now have access to an intermediate representation that we can edit and modify *without* re-training. Given an input image, we fully encode the image and generate Gaussians that we splat to reconstruct the image. First, we evaluate the image reconstruction quality of our model. On the ImageNet validation set, our ViT-base model achieved 89.45 on reconstruction FID, while the MAE ViT-base model got 98.12 (lower is better). This improvement in reconstruction quality is due to the non-uniformity of the learned distribution of Gaussians, which allows GMAE to model high-frequency information, as shown in Fig. 5. As a result, our reconstructions can be used directly for other tasks without needing to add a GAN loss or an upsampling layer on top.

Another advantage of using a 3D Gaussian representation to represent 2D images is that it learns to separate objects in the z direction. This may be due to the fact that with random initialization, the points closer to the camera represent low-frequency information, while the points far from the camera model the high-frequency information (see Section 4.4). To segment an image along the z axis, we simply sort the predicted Gaussians based on their depth value and group them into $L = l_0, l_1, ...l_d$ groups. To split an image into two layers, we try to render it as two images using $l_0, ..., l_n$ and $l_0, ..., l_n, l_{n+1}$. If the difference at a pixel is larger than a specific threshold th, we assign that pixel to the layer $n + 1$. Fig. 6 shows the layering effect of a Gaussian representation with 64 layers. We also show the layering effect in pixel space in Fig. 7.

Zero-shot Figure-Ground Separation: The layer-wise rendering allows us to perform figure-ground segmentation for free. We simply get the layer-wise rendered image and apply a threshold to obtain foreground-background segmentation. We evaluate our approach on the PASCAL dataset (Everingham et al., 2015) on foreground segmentation and single object detection tasks as in (Bar et al., 2022) (see Table 3). The "copy" baseline (Bar et al., 2022) predicts a random ground truth mask from the training set. We note that GMAE performs better than other few-shot baselines despite being a zero-shot approach.
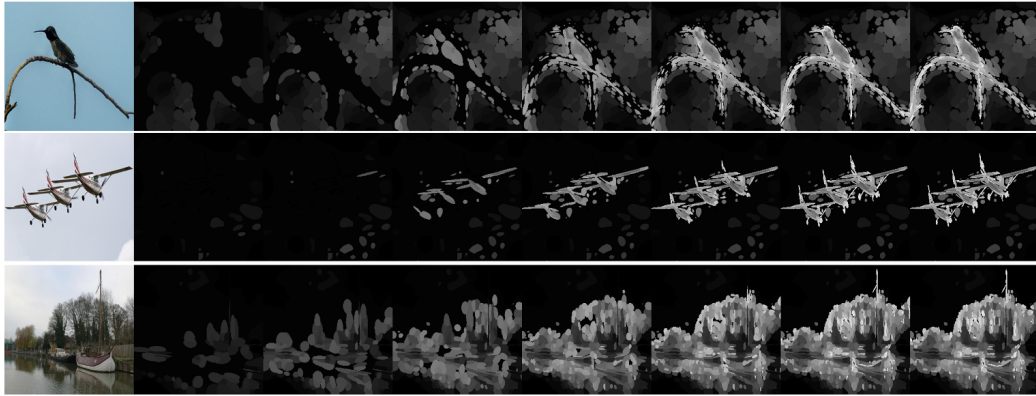
Figure 6: **Visualization of Gaussian layers:** The first column shows the RGB input image, and the subsequent columns show the Gaussian layers in inverse-depth ordering. The layer-wise rendering highlights the model's ability to separate objects and represent them in distinct frequency layers, enabling zero-shot foreground-background segmentation and edge detection.

Figure 7: **Visualization of Gaussian layers on RGB:** The first column shows the RGB input image, and the rest of the columns show rendering of partial depth Gaussians. We select first K Gaussians from all the Gaussians after sorting based on depth. Then we only render these K Gaussians. The Figure shows $K = 32, 64, 128, 256, 512, 1024$, and the last being fully rendered image using all Gaussians.

Zero-shot Edge detection: In a similar fashion, as in zero-shot figure-ground segmentation, we can simply take the layer-wise rendered image and find edges with a discontinuity in the z direction. Additionally, the number of layers determines the granularity in the edge detection; for example, a large number of layers means we will detect more fine-grained edges. Fig. 9 shows the detected edges of our zero-shot method with varying number of layers. We also quantitatively evaluate our method on BSDS500 (Arbelaez et al., 2010). Table 4 shows that our method archives reasonable performance for zero-shot detection without ever being trained for segmentation or detection. Fig. 8 shows that as we decrease the number of layers (*e.g.*, increasing the width of each layer), the quality of edge detection gets better, allowing us to have a hierarchy of edges.

8

Model	Foreground Segmentation ↑				Single Object Detection ↑
	Split 0	Split 1	Split 2	Split 3	
Copy (Bar et al., 2022)	12.92	17.90	13.52	15.29	13.50
BEiT (Bao et al., 2021)	0.38	0.93	0.90	0.95	0.32
VQGAN (Esser et al., 2020)	6.96	10.55	9.59	9.43	4.99
MAE (He et al., 2022)	1.92	6.76	3.85	4.57	1.98
MAE-VQGAN (Bar et al., 2022)	2.22	7.07	5.48	6.28	3.21
GMAE	17.85	19.09	19.16	16.55	20.26

Table 3: **Zero shot segmentation and detection:** We evaluate on a random subset of the PAS-CAL (Everingham et al., 2015) dataset for figure-ground segmentation and single object detection.

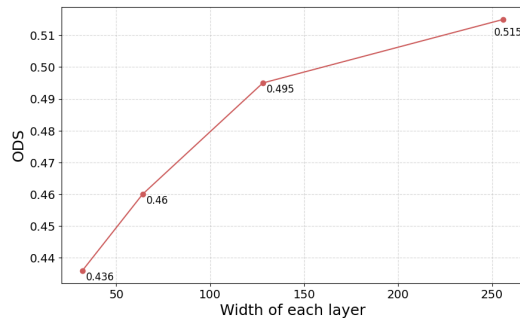| Method	ODS	OIS	AP
HED	0.788	0.808	0.840
EDETR	0.840	0.858	0.896
Zero-shot:			
Sobel filter	0.539	-	-
Canny	0.600	0.640	0.580
Felz-Hutt	0.610	0.640	0.560
SAM	0.768	0.786	0.794
GMAE	0.515	0.524	0.248

Table 4: **Zero-shot transfer to edge detection:** on BSDS500 (Arbelaez et al., 2010).

Figure 8: **Edge Detection:** quality improves as we increase the width of each layer.
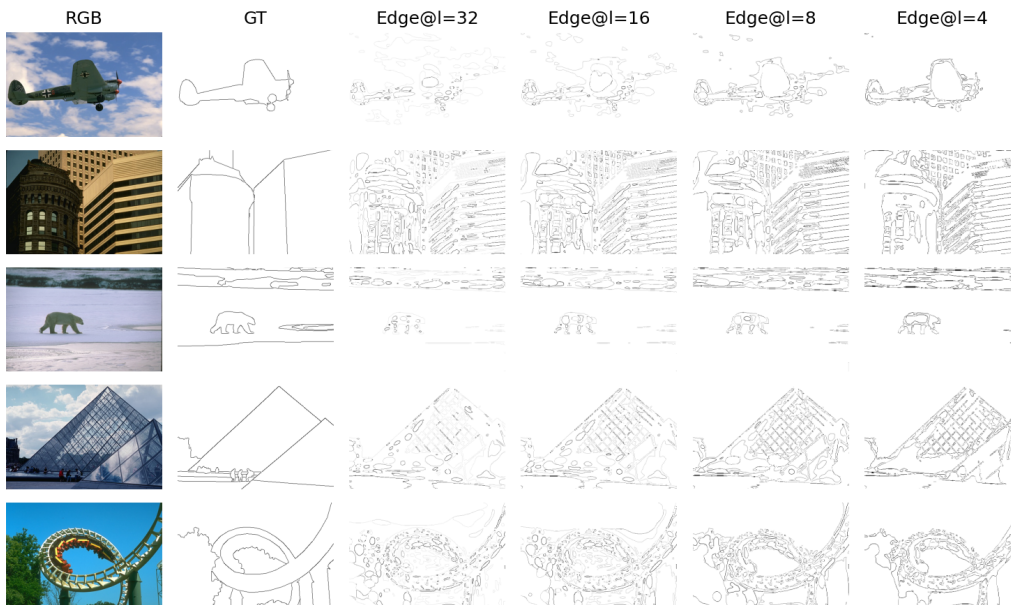

Figure 9: **Zero-shot Edge Detection:** Gaussians from our decoder are grouped into equal sets of layers, based on their depth ordering. Then we render each layer one by one and update the pixel if adding that layer makes significant change in that pixel. From this layered image, we simply find edges if there is a discontinuity from one layer to another. We can get a hierarchy of edges by decreasing the number of layers (or increasing the width of a layer). These results are on BSDS500 (Arbelaez et al., 2010). *l*@16 means we have a total of 16 uniformly grouped layers.

Figure 11: **Distribution of Gaussians on xy-plane:** We plot the xy position of Gaussian centers along with their opacity values. Unlike patches, Gaussians are positioned dynamically based on the image. For example, in the 4th image, Gaussians are arranged in a circular pattern, while in the 2nd image there arranged as a rectangle. This degree of freedom allows them to add high-frequency signals to the image, by concentrating more Gaussians to those regions.

4.4 Qualitative Results

Distribution of Gaussians in xy: Fig. 11 shows how the Gaussians are arranged differently in space for different images. In patch-based methods such as MAE, patches are arranged in a uniform tile. Even if we decrease the patch size to increase the number of patches, they will still be uniformly allocated across all regions. However, in our work, a Gaussian can go to any part of the image, which allows them to dynamically position themselves based on the input image. This property allows modeling high-frequency regions with high fidelity. As shown in Fig. 5, our reconstructions can capture high-frequency regions such as faces and intricate patterns.

Size vs Depth: Fig. 10 shows a clear trend: the Gaussians with larger scale values lie closer to the camera, while the ones with smaller scale values, lie away from the camera, on average. This distribution validates our previous hypothesis in Sec 4.3, that low-frequency blobs lie closer and cover larger regions, while high-frequency blobs lie away from the camera, on average. At the start, some Gaussians will be closer to the camera, influencing more pixels, therefore representing low-frequency regions. Our layering results are the outcome of this property. In the real world, backgrounds tend to have low-frequency regions while objects usually have high-frequency details. This correlation leads to our zero-shot results. We attribute this to, as all else, to divine benevolence.
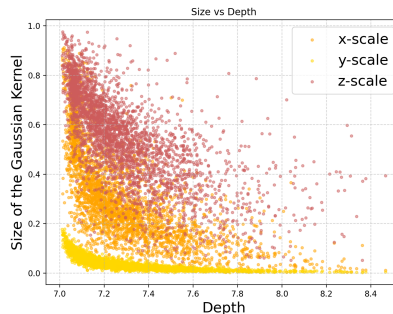

Figure 10: **Size vs. Depth:** Distribution of factorized scale values (s) over predicted depth.

5 Discussion

This paper presents GMAE, a self-supervised image representation learning approach that extends MAE to include a learned intermediate Gaussian representation to jointly learn semantics and spatial understanding. We show that learning to represent images with 3D Gaussians has several built-in advantages that stem from their non-uniform dynamical allocation of scale, location, and distribution. Our method, therefore, lends itself to zero-shot capabilities of spatial understanding such as foreground-background segmentation, image layering, and edge detection. Along with these advantages, we demonstrate that the representation learned by our method is still has good semantic abstractions, and is on par with MAE on standard supervised image recognition tasks and that it transfers to downstream tasks such as detection and segmentation via fine-tuning.

GMAE still exhibits several empirical limitations. For example, setting larger scale values at the start of training results in a more challenging optimization. Compared to the number of Gaussians typically used for 3D reconstructions (up to millions), the number of Gaussians we have used in GMAE is bottlenecked by compute, and increasing it to more than a thousand can cause major slow-downs for pre-training. An interesting future direction is to further accelerate our pipeline.

We hope our exploration can inspire more work in this direction and truly unlock the next generation of techniques that effectively model visual data.

REFERENCES

Pablo Arbelaez, Michael Maire, Charless Fowlkes, and Jitendra Malik. Contour detection and hierarchical image segmentation. *IEEE TPAMI*, 33(5):898–916, 2010.

Hangbo Bao, Li Dong, Songhao Piao, and Furu Wei. Beit: Bert pre-training of image transformers. *arXiv preprint arXiv:2106.08254*, 2021.

Amir Bar, Yossi Gandelsman, Trevor Darrell, Amir Globerson, and Alexei Efros. Visual prompting via image inpainting. *Advances in Neural Information Processing Systems*, 35:25005–25017, 2022.

Jonathan T Barron, Ben Mildenhall, Dor Verbin, Pratul P Srinivasan, and Peter Hedman. Mip-nerf 360: Unbounded anti-aliased neural radiance fields. In *Proceedings of the IEEE/CVF Conference on Computer Vision and Pattern Recognition*, pp. 5470–5479, 2022.

Mathilde Caron, Hugo Touvron, Ishan Misra, Hervé Jégou, Julien Mairal, Piotr Bojanowski, and Armand Joulin. Emerging properties in self-supervised vision transformers. In *Proceedings of the IEEE/CVF international conference on computer vision*, pp. 9650–9660, 2021.

Ting Chen, Simon Kornblith, Mohammad Norouzi, and Geoffrey Hinton. A simple framework for contrastive learning of visual representations. In *International conference on machine learning*, pp. 1597–1607. PMLR, 2020.

Jia Deng, Wei Dong, Richard Socher, Li-Jia Li, Kai Li, and Li Fei-Fei. Imagenet: A large-scale hierarchical image database. In *2009 IEEE conference on computer vision and pattern recognition*, pp. 248–255. Ieee, 2009.

Jacob Devlin, Ming-Wei Chang, Kenton Lee, and Kristina Toutanova. Bert: Pre-training of deep bidirectional transformers for language understanding. *arXiv preprint arXiv:1810.04805*, 2018.

Alexey Dosovitskiy, Lucas Beyer, Alexander Kolesnikov, Dirk Weissenborn, Xiaohua Zhai, Thomas Unterthiner, Mostafa Dehghani, Matthias Minderer, Georg Heigold, Sylvain Gelly, et al. An image is worth 16x16 words: Transformers for image recognition at scale. *arXiv preprint arXiv:2010.11929*, 2020.

Patrick Esser, Robin Rombach, and Björn Ommer. Taming transformers for high-resolution image synthesis. 2021 ieee. In *CVF Conference on Computer Vision and Pattern Recognition (CVPR)*, pp. 12868–12878, 2020.

Mark Everingham, SM Ali Eslami, Luc Van Gool, Christopher KI Williams, John Winn, and Andrew Zisserman. The pascal visual object classes challenge: A retrospective. *International journal of computer vision*, 111:98–136, 2015.

Jean-Bastien Grill, Florian Strub, Florent Altché, Corentin Tallec, Pierre Richemond, Elena Buchatskaya, Carl Doersch, Bernardo Avila Pires, Zhaohan Guo, Mohammad Gheshlaghi Azar, et al. Bootstrap your own latent-a new approach to self-supervised learning. *Advances in neural information processing systems*, 33:21271–21284, 2020.

Kaiming He, Xiangyu Zhang, Shaoqing Ren, and Jian Sun. Deep residual learning for image recognition. arxiv e-prints. *arXiv preprint arXiv:1512.03385*, 10, 2015.

Kaiming He, Haoqi Fan, Yuxin Wu, Saining Xie, and Ross Girshick. Momentum contrast for unsupervised visual representation learning. In *Proceedings of the IEEE/CVF conference on computer vision and pattern recognition*, pp. 9729–9738, 2020.

Kaiming He, Xinlei Chen, Saining Xie, Yanghao Li, Piotr Dollár, and Ross Girshick. Masked autoencoders are scalable vision learners. In *Proceedings of the IEEE/CVF conference on computer vision and pattern recognition*, pp. 16000–16009, 2022.

Varun Jampani, Deqing Sun, Ming-Yu Liu, Ming-Hsuan Yang, and Jan Kautz. Superpixel sampling networks. In *Proceedings of the European Conference on Computer Vision (ECCV)*, pp. 352–368, 2018.

Chao Jia, Yinfei Yang, Ye Xia, Yi-Ting Chen, Zarana Parekh, Hieu Pham, Quoc Le, Yun-Hsuan Sung, Zhen Li, and Tom Duerig. Scaling up visual and vision-language representation learning with noisy text supervision. In *International conference on machine learning*, pp. 4904–4916. PMLR, 2021.

Bernhard Kerbl, Georgios Kopanas, Thomas Leimkühler, and George Drettakis. 3d gaussian splatting for real-time radiance field rendering. *ACM Transactions on Graphics*, 42(4):1–14, 2023.

Diederik P Kingma. Auto-encoding variational bayes. *arXiv preprint arXiv:1312.6114*, 2013.

Alex Krizhevsky, Ilya Sutskever, and Geoffrey E Hinton. Imagenet classification with deep convolutional neural networks. *Advances in neural information processing systems*, 25, 2012.

Christoph Lassner and Michael Zollhöfer. Pulsar: Efficient sphere-based neural rendering. In *IEEE/CVF Conference on Computer Vision and Pattern Recognition (CVPR)*, June 2021.

Marc Levoy. Efficient ray tracing of volume data. *ACM Transactions on Graphics (ToG)*, 9(3): 245–261, 1990.

Tianhong Li, Huiwen Chang, Shlok Mishra, Han Zhang, Dina Katabi, and Dilip Krishnan. Mage: Masked generative encoder to unify representation learning and image synthesis. In *CVPR*, 2023.

Yanghao Li, Hanzi Mao, Ross Girshick, and Kaiming He. Exploring plain vision transformer backbones for object detection. In *European Conference on Computer Vision*, pp. 280–296. Springer, 2022.

Tsung-Yi Lin, Michael Maire, Serge Belongie, James Hays, Pietro Perona, Deva Ramanan, Piotr Dollár, and C Lawrence Zitnick. Microsoft coco: Common objects in context. In *Computer Vision– ECCV 2014: 13th European Conference, Zurich, Switzerland, September 6-12, 2014, Proceedings, Part V 13*, pp. 740–755. Springer, 2014.

Shichen Liu, Tianye Li, Weikai Chen, and Hao Li. Soft rasterizer: A differentiable renderer for image-based 3d reasoning. In *Proceedings of the IEEE/CVF international conference on computer vision*, pp. 7708–7717, 2019.

Francesco Locatello, Dirk Weissenborn, Thomas Unterthiner, Aravindh Mahendran, Georg Heigold, Jakob Uszkoreit, Alexey Dosovitskiy, and Thomas Kipf. Object-centric learning with slot attention. *Advances in neural information processing systems*, 33:11525–11538, 2020.

Ilya Loshchilov and Frank Hutter. Decoupled weight decay regularization. *arXiv preprint arXiv:1711.05101*, 2017.

Ben Mildenhall, Pratul P Srinivasan, Matthew Tancik, Jonathan T Barron, Ravi Ramamoorthi, and Ren Ng. Nerf: Representing scenes as neural radiance fields for view synthesis. *Communications of the ACM*, 65(1):99–106, 2021.

Maxime Oquab, Timothée Darcet, Théo Moutakanni, Huy V. Vo, Marc Szafraniec, Vasil Khalidov, Pierre Fernandez, Daniel HAZIZA, Francisco Massa, Alaaeldin El-Nouby, Mido Assran, Nicolas Ballas, Wojciech Galuba, Russell Howes, Po-Yao Huang, Shang-Wen Li, Ishan Misra, Michael Rabbat, Vasu Sharma, Gabriel Synnaeve, Hu Xu, Herve Jegou, Julien Mairal, Patrick Labatut, Armand Joulin, and Piotr Bojanowski. DINOv2: Learning robust visual features without supervision. *Transactions on Machine Learning Research*, 2024. ISSN 2835-8856. URL https://openreview.net/forum?id=a68SUt6zFt. Featured Certification.

Alec Radford, Jong Wook Kim, Chris Hallacy, Aditya Ramesh, Gabriel Goh, Sandhini Agarwal, Girish Sastry, Amanda Askell, Pamela Mishkin, Jack Clark, et al. Learning transferable visual models from natural language supervision. In *International conference on machine learning*, pp. 8748–8763. PMLR, 2021.

Ilija Radosavovic, Tete Xiao, Stephen James, Pieter Abbeel, Jitendra Malik, and Trevor Darrell. Real-world robot learning with masked visual pre-training. In *Conference on Robot Learning*, 2022.

Robin Rombach, Andreas Blattmann, Dominik Lorenz, Patrick Esser, and Björn Ommer. High-resolution image synthesis with latent diffusion models. In *Proceedings of the IEEE/CVF conference on computer vision and pattern recognition*, pp. 10684–10695, 2022.

Richard Tucker and Noah Snavely. Single-view view synthesis with multiplane images. In *Proceedings of the IEEE/CVF Conference on Computer Vision and Pattern Recognition*, pp. 551–560, 2020.

Ashish Vaswani, Noam Shazeer, Niki Parmar, Jakob Uszkoreit, Llion Jones, Aidan N Gomez, Łukasz Kaiser, and Illia Polosukhin. Attention is all you need. *Advances in neural information processing systems*, 30, 2017.

John YA Wang and Edward H Adelson. Representing moving images with layers. *IEEE transactions on image processing*, 3(5):625–638, 1994.

Chen Wei, Haoqi Fan, Saining Xie, Chao-Yuan Wu, Alan Yuille, and Christoph Feichtenhofer. Masked feature prediction for self-supervised visual pre-training. In *Proceedings of the IEEE/CVF Conference on Computer Vision and Pattern Recognition*, pp. 14668–14678, 2022.

Zhirong Wu, Yuanjun Xiong, Stella X Yu, and Dahua Lin. Unsupervised feature learning via non-parametric instance discrimination. In *Proceedings of the IEEE conference on computer vision and pattern recognition*, pp. 3733–3742, 2018.

Yufei Xu, Jing Zhang, Qiming Zhang, and Dacheng Tao. ViTPose: Simple vision transformer baselines for human pose estimation. In *Advances in Neural Information Processing Systems*, 2022.

Yang You, Igor Gitman, and Boris Ginsburg. Large batch training of convolutional networks. *arXiv preprint arXiv:1708.03888*, 2017.

Yuhao Zhang, Hang Jiang, Yasuhide Miura, Christopher D Manning, and Curtis P Langlotz. Contrastive learning of medical visual representations from paired images and text. In *Machine Learning for Healthcare Conference*, pp. 2–25. PMLR, 2022.

Tinghui Zhou, Richard Tucker, John Flynn, Graham Fyffe, and Noah Snavely. Stereo magnification: Learning view synthesis using multiplane images. *arXiv preprint arXiv:1805.09817*, 2018.

Adrian Ziegler and Yuki M Asano. Self-supervised learning of object parts for semantic segmentation. In *Proceedings of the IEEE/CVF Conference on Computer Vision and Pattern Recognition*, pp. 14502–14511, 2022.

A TRAINING DETAILS

Here we provide configurations used for training 5 and finetuning 6 our models. For pre-training, we follow a similar recipe as in MAE (He et al., 2022). For linear probing we use AdamW instead of LARS (You et al., 2017) as in MAE (He et al., 2022).

Config	Value
optimizer	AdamW (Loshchilov & Hutter, 2017)
base learning rate	1e-4
minimum absolute lr	0.0
weight decay	0.05
optimizer momentum	$\beta_1 = 0.9, \beta_2 = 0.95$
batch size	4096
learning rate schedule	cosine decay (Loshchilov & Hutter, 2017)
warmup epochs	20
training epochs	400
augmentation	RandAug (9, 0.5)
label smoothing	0.1
mixup	0.0
cutmix	0.0
drop path	0
layer decay	1.0

Table 5: **Pre-training recipe for GMAE**.

Config	Value
optimizer	AdamW (Loshchilov & Hutter, 2017)
base learning rate	1e-4
minimum absolute lr	0.0
weight decay	0.01
optimizer momentum	$\beta_1 = 0.9, \beta_2 = 0.999$
batch size	4096
learning rate schedule	linear decay
warmup epochs	10
training epochs	90
augmentation	BasicAug
label smoothing	0.1
mixup	0.8
cutmix	0.5
drop path	0.2
layer decay	0.8

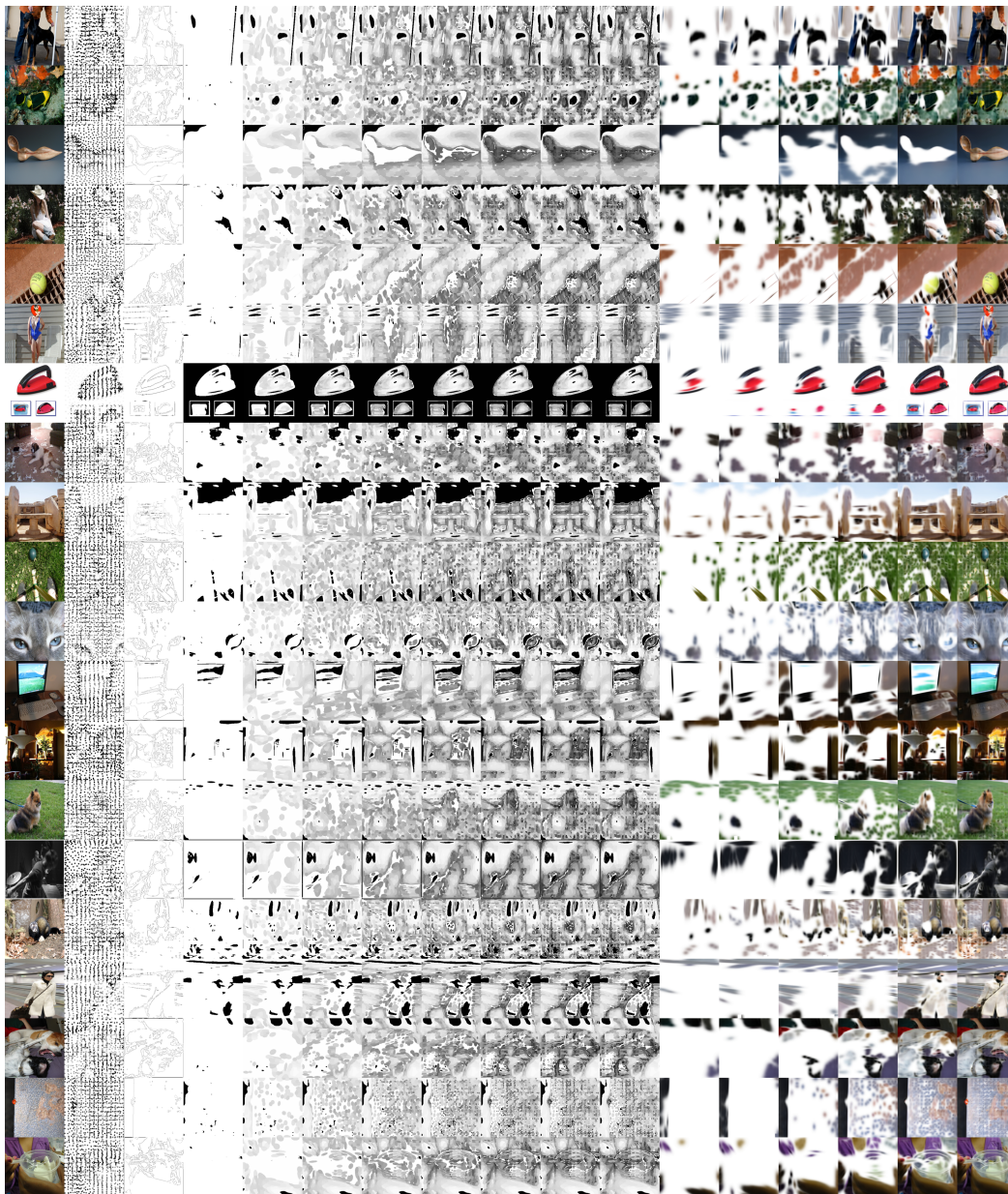Table 6: **Fine tuning recipe GMAE**.

Figure 12: **Unfiltered Samples:** We show more samples from ImageNet-1K, which RGB, XY positions of Gaussians, layering of Gaussians, and RGB layering.